



Prototype Si microstrip sensors for the CDF-II ISL detector

K. Hara^{a,*}, K. Hata^a, K. Kanao^a, S. Kim^a, M. Ogasawara^a, T. Ohsugi^b,
M. Shimojima^a, K. Takikawa^a

^aUniversity of Tsukuba, Institute of Physics, Tsukuba, Ibaraki 305-8571, Japan

^bDepartment of Physics, Hiroshima University, Higashi-Hiroshima, Hiroshima 739-8526, Japan

Received 17 May 1999

Abstract

Prototype Si microstrip sensors for the CDF-II ISL were fabricated by Hamamatsu Photonics and SEIKO Instruments using 4" technology. The sensor is AC coupled and double-sided forming a stereo angle of 1.207°. The strip pitch is 112 μm on both sides. The main differences between the two manufacturers lie on the technologies of passivation and the structure of coupling capacitors. We describe the design of the sensor and evaluation results of the performance. The evaluations include the total and individual strip currents and interstrip capacitance measured before and after ⁶⁰Co γ irradiation. © 1999 Elsevier Science B.V. All rights reserved.

1. Introduction

The CDF detector at Fermilab Tevatron is currently being upgraded to CDF-II [1] in order to take full advantage of 10-fold increase in luminosity. One of the major upgrades is the replacement of the entire central tracking system; the new system will consist of five layers of double-sided Si microstrip detectors, SVX-II ($2.5 < r < 10.6$ cm), the intermediate radius Si layers, ISL ($20 < r < 30$ cm), and the central open cell tracker, COT ($46 < r < 131$ cm). Combining the measurements with SVX-II and ISL allows precision standalone tracking with up to seven axial and seven stereo measurements.

The ISL is constructed from five barrels in total; one central barrel, inner and outer barrels at forward and backward regions. The Si sensors are AC-coupled and double-sided with the electrode strips forming a small stereo angle of $\sim 1.2^\circ$. Each barrel has single layer of such Si sensors arranged into ladders, each ladder consisting of six Si microstrip sensors lined along the beam direction. The strips of three Si sensors in a ladder are wire-bonded so that the signals can be read out from either end of the ladder. Each barrel is composed of 28, 24 and 36 such ladders for the central, inner and outer forward/backward barrels. The total numbers thus count to 148 ladders and 888 Si sensors. About a half of the sensors are fabricated using 4" technology. We describe the prototype of these sensors.

Four-inch ISL prototype sensors have been fabricated by Hamamatsu Photonics Co. (HPK) and SEIKO Instruments Inc. (SII). The sensitive area is

*Corresponding author. Tel.: + 81-298-53-4270; fax: + 81-298-53-4491.

E-mail address: hara@hep.px.tsukuba.ac.jp (K. Hara)

57.23 mm wide and 67.5 mm long with a thickness of 300 μm . The p-side strips have small stereo angle of 1.207° with respect to the n-side strips which run parallel to the longer side. To compromise between the number of readout channels and the required spatial resolution, the strip pitch was determined to be 112 μm with the number of readout strips being 512 per side.

2. Prototype design

2.1. Strip width considerations

The prototype sensor design is based on the HPK Si microstrip sensor developed for the SDC [2]. Given the strip pitch of 112 μm , the implant strip width and Al electrode width are chosen to be 22 and 16 μm ; the Al electrode is recessed by 3 μm from the implant strip edges. This design reduces the electric field strength in the bulk in the vicinity of the implant strip edges, which helps to reduce the micro-discharge [3]. The implant strip width is determined from a compromise of effects on the full depletion voltage, the detector capacitance, and Al electrode resistivity, the latter two contributing to the amplifier noise. With increasing the strip width, the detector capacitance increases while the full depletion voltage and the Al electrode resistivity decreases. Because of fringing fields near the strip structures, excess bias voltages are necessary for strip detectors compared to simple diodes in order to be fully depleted, which is discussed in Ref. [4]. There are several measurements available [5–7] of the dependence of the full depletion voltage on the strip width for double-sided Si detectors. Although the measured excess voltages are slightly smaller than the calculation [4], they tend to become substantially high for strip widths narrower than $\sim 20\%$ of the strip pitch.

The interstrip capacitance on the p-side is well studied and can be expressed approximately by $(0.75 + 1.8W/P)$ pF/cm [5] for strip width of W and pitch P , which gives 1.0 pF/cm for our sensors. We note that the measured value is $1.2^{+0}_{-0.15}$ pF/cm (0.15 being the estimate of the stray capacitance) for both HPK and SII sensors, and is consistent with this empirical formula.

The n strips in n-bulk have a larger capacitance than p strips since the charge accumulated between n strips makes the n electrode effectively wider. Implantation of p^+ between n strips, or p-stop, is for the purpose of isolating n strips. We employed the individual p-stop configuration [6] where each n strip is surrounded by floating p^+ . The region between the neighboring n strips is covered as much as possible by p-stop implants, leaving a gap of 8 μm between the neighboring p-stop implants and 10 μm between the n^+ and p-stop. The n-side capacitance is studied by the RD20 group [8,9] both in the individual configuration and in the common configuration where all the p-stop implants are connected together beyond the strip ends. According to their study, the interstrip capacitance is slightly smaller in the individual configuration. Although RD20 quotes an n-side capacitance of ~ 2 pF/cm, it is known to decrease further with the bias voltage. Our capacitance measurement is described in Section 3.

The signal is read out with SVX3 chips whose integrator is essentially a double cascode configuration with a PMOS input transistor [10]. Among the various noise contributions (see, for example, [11]), we compared the FET Johnson noise and the thermal noise from the series input resistance in order to evaluate the influence of the Al electrode resistance and detector capacitance. The two factors contribute to the noise charge through

$$(\text{Noise charge})^2 \sim 4kTC_D^2 \left(R_{\text{eff}} + \frac{2}{3} \frac{1}{g_m} \right) \quad (1)$$

where k is the Boltzmann constant, C_D the detector capacitance, g_m the transconductance, and R_{eff} the effective resistance input to the preamplifier. The signal picked up by the Al electrode is transmitted through an RC chain whose effective resistance is $\frac{1}{3}$ of the actual Al electrode resistance in the frequency region concerned. The measured Al electrode resistivity is 12 Ω/cm for HPK and 13 Ω/cm for SII. Under these conditions and other parameters taken as inputs, a calculation resulted in that the noise at a strip width of 22 μm is located at minimum in the wide parameter range considered.

2.2. Other designs common to the manufacturers

A single guard ring structure is employed. In order to reduce the insensitive area, the p^+ guard ring on the p-side is located underneath the bias ring and its potential is held to the bias voltage. Similarly, the n^+ guard ring on the n-side is located underneath and DC connected to the bias ring. A pair of floating p-stop rings are located inside and outside the n^+ guard ring for isolation.

The bias voltage to individual implant strips is provided by polycrystalline silicon (poly-Si) resistors with a mean resistance of 4 M Ω . The poly-Si with a width of 5 μm and a unit resistance of ~ 1 M Ω/mm (HPK) or ~ 1.5 M Ω/mm (SII) is placed inside the guard ring making several turns. While the Al electrodes are terminated not to overlap with the poly-Si resistors, the implant strips are extended underneath the poly-Si towards the guard ring. Charge accumulated by the strips in this region can still be picked up by the Al electrodes. This design therefore allows the region inside the bias ring to be fully efficient; The distance between the scribed edge and the bias ring is 700–750 μm .

A single row of bonding pads, 200 \times 60 μm , are located 1.7 mm from the detector end on the poly-Si resistor side. The pads at the other side are located at 1.0 mm. On the stereo side, 12 short strips which are not read out are biased from the end opposite to the readout strips.

2.3. Designs specific to the manufacturers

Although the geometrical design is similar, the coupling capacitors, passivation, and edge treatments are specific to the manufacturers.

The coupling capacitor of HPK sensors has a double-layer structure of SiO_2 and Si_3N_4 developed by chemical vapor deposition. The double-layer structure helps to reduce creation of pinholes. The thicknesses are 0.2 and 0.1 μm , respectively, which achieved a coupling capacitance of 19 pF/cm (measured value). The passivation is SiO_2 .

The main feature of the SII process is the ONO (oxide–nitride–oxide) coupling capacitor structure with the LOCOS (local oxidation silicon) process [12–14] (see Fig. 1). A layer of LOCOS SiO_2 is developed first keeping its thickness reduced at the strip positions, where n^+ and p^+ strips are implanted underneath by ion bombardment. The coupling capacitor is an ONO strip consisting of 0.15 μm thick Si_3N_4 sandwiched by 0.04 and ~ 0.005 μm thick SiO_2 layers. On top of the ONO strip located is a strip of poly-Si which is DC coupled to the Al electrode. The ONO coupling structure can provide a large coupling capacitance, which was measured to be 25 pF/cm. The surface is finally passivated by P-SiN (SiN passivation deposited by plasma enhanced chemical vapor deposition). Although the structure employed by SII looks complicated in comparison with the HPK structure, the processes are commonly available in conventional CMOS technology.

HPK employed an n^+ scribe line implant and Al covering the oxide layer on top, which eliminates variation in the charge on the oxide surface and reduces the effects from the scribed edges. In the SII design, no such structures were instrumented and the region outside the guard ring is kept clear.

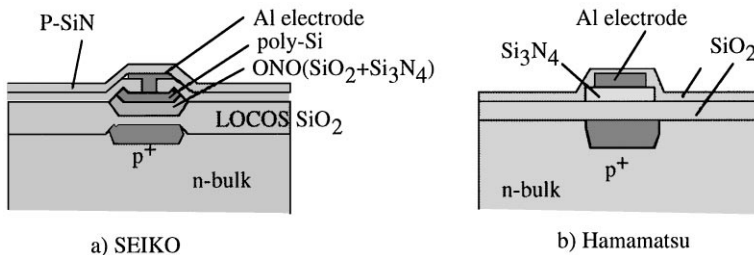


Fig. 1. Passivation and coupling capacitor of (a) SII and (b) HPK sensors.

3. Performance

3.1. Leakage current

Fig. 2 compares the total leakage current of some of HPK and SII sensors. The full depletion voltage defined from C - V curves is about 90 V for HPK and 55 V for SII sensors. We specify the leakage current be less than 4 μA at the operation voltages, defined as 10 V above the full depletion voltages. The HPK sensors showed a leakage current well under the specification. The total leakage current of SII sensors was about one order higher than that of HPK sensors at the operation voltages, which still satisfies the specification. We note that the I - V characteristics vary among the production batches. Though the leakage current of SII sensors shown in the figure increases gradually above the full depletion voltage, many other SII sensors showed a steep increase above 100–120 V. On the other hand, some other HPK sensors showed no steep increase up to 200 V. Along with the specification on the total leakage current, we require that the current increase above the full depletion voltage be small in order to assure no such steep increase exists in the voltage range below 100 (SII) or 160

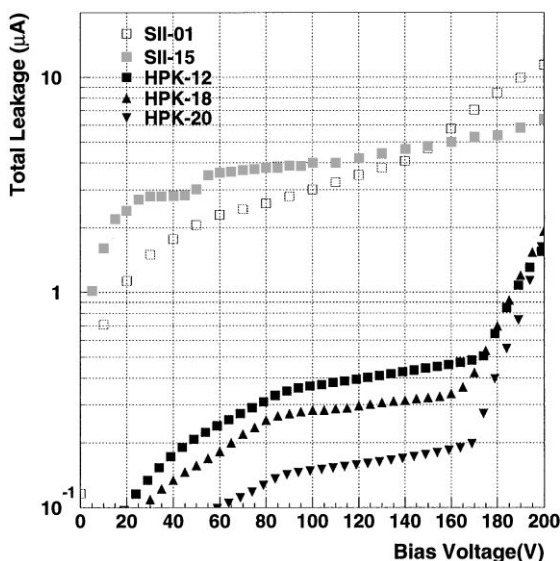


Fig. 2. Total leakage current as a function of bias voltage. HPK and SII sensors are compared.

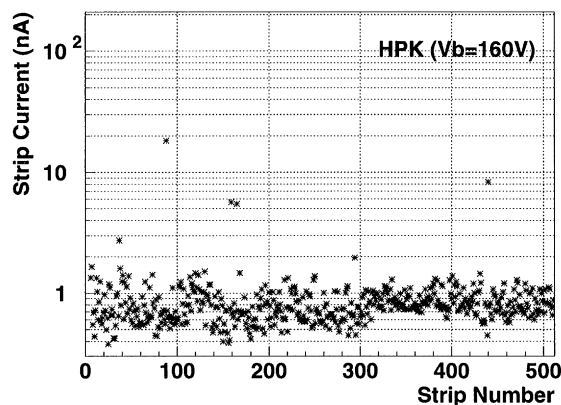


Fig. 3. Strip leakage current of HPK sensor #18 at 160 V.

V (HPK). The leakage current of the delivered 10 HPK sensors ranged from 0.2 to 1.8 μA (0.8 μA on average) at 160 V, and that of 8 delivered SII sensors ranged from 2.5 to 26 μA (10 μA on average) at 100 V.

In order to investigate the reasons for the increase of the leakage current, individual strip leakage currents were measured by probing the DC pads instrumented on the implant strips and measuring the induced current across the probe and the bias ring on the side under evaluation. The strip leakage currents measured on the p-strip side are plotted in Figs. 3 and 4 against the strip number. The data shown were taken at 160 V for HPK, and at 100 V for SII. There are some leaky strips evident especially for the SII sensor. The SII sensor in the plot showed a steep increase in the leakage current above 100 V, and the leaky strips are apparently responsible for this increase. Similar tendency was observed for other sensors and also for HPK sensors measured at bias voltage where the leakage current starts to increase steeply. We also confirmed with an infrared CCD camera that IR lights are emitted locally near strip edges. From these observations we attribute the steep current increase to a number of strips which draw larger currents due to micro-discharge.

The location of leaky strips is not identical among the different sensors, which eliminates the possibility of errors in the masks. We have experienced that HPK single-sided p-strip-type sensors showed such a steep current increase much less

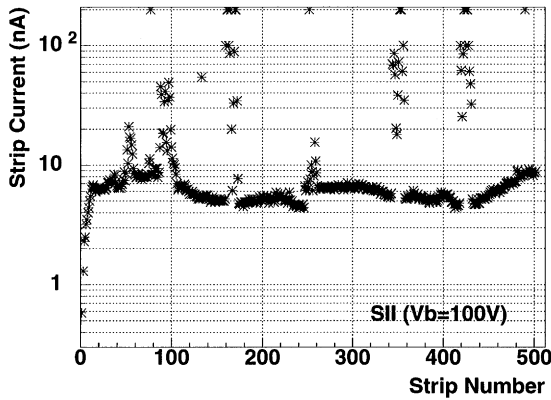


Fig. 4. Strip leakage current of SII sensor #22 at 100 V. The strip currents of more than 200 nA are truncated and plotted at 200 nA.

frequently while single-sided n-strip-type sensors showed micro-discharges. As far as the HPK process is concerned, leaky strips probably originate in the n-side process such as p-stop processing. Definitive conclusion is, however, difficult since quality monitoring is not possible until the final passivation process is completed.

The strip current of quiet channels is ~ 1 nA for HPK and 5–8 nA for SII, which explains the total leakage current difference at operation voltage. It is pointed out [3,15] that the additional layer of silicon nitride increases the total leakage current, and [16] that etching off Si_3N_4 in the region between the strips prevents an increase of the leakage current. The present observation implies that etching off Si_3N_4 does not reduce the leakage current to the level a single SiO_2 layer can achieve, although we cannot conclude definitively since the difference might lie on the process quality of the two manufacturers.

3.2. Interstrip capacitance

The n-side interstrip capacitance was evaluated by probing the AC bonding pads and using an HP4275A LCR meter. The interstrip capacitance is defined as the capacitance between one central strip to the next neighboring Al electrodes on both sides while others are floating. The data are taken as a function of bias voltage at various LCR meter

frequencies, ranging from 100 kHz to 10 MHz. The interstrip capacitance is characterized better at higher LCR frequencies since the bias resistors exist in parallel in the circuit. We measured that the interstrip capacitance is not affected by the frequency choice in this frequency range in the bias voltage region above the full depletion. Typical data are shown in Section 3.3, where we discuss the irradiation effects. The n-side interstrip capacitance was 9 pF/strip at the operation voltages. The contribution from other strips was measured to be ~ 1 pF. We therefore can achieve an n-side capacitance of 30 pF when three sensors are wire bonded.

3.3. Performance to ^{60}Co γ 's irradiation

The ISL sensors will not receive more than 0.1 Mrad of radiation for an integrated Tevatron luminosity of 10 fb^{-1} . Taking these conditions into account, we measured the electrical properties one week after the irradiation of 0.16 Mrad ^{60}Co γ -rays. We require that the total leakage current be less than 120 μA and no major changes be present in electrical properties. Although the substantial part of the radiation at the Tevatron is due to hadrons, we conducted a ^{60}Co irradiation test to investigate the difference of surface conditions between the two manufacturers; effects to the bulk are studied elsewhere [17].

The irradiation was performed at the ^{60}Co γ -ray irradiation facility of the Japan Atomic Energy Research Institute (JAERI). The sensor was held in a test frame with ~ 60 electrodes and bias-rings wire-bonded to electrodes printed on the frame. Four sensors, two of each manufacturer, were irradiated. The irradiation was interrupted at accumulated doses of 7, 35 and 160 krad while the I - V characteristics were measured without the ^{60}Co source. The temperature of the irradiation cave was 17°C . The interstrip and bulk capacitances were measured before and one week after the irradiation of 0.16 Mrad.

Fig. 5 shows the leakage currents versus the elapsed time of two SII sensors and the average of two HPK sensors. The data points correspond to the last two irradiation periods and the intermission in between. The current readings of three of the

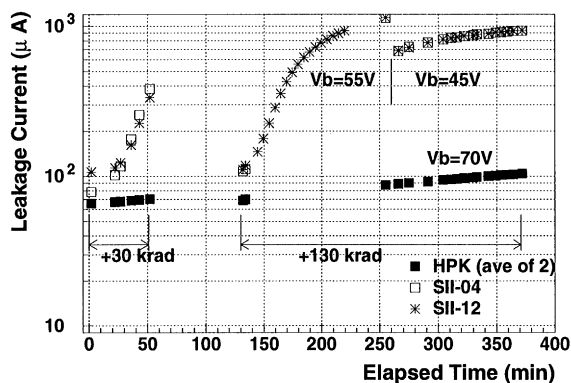


Fig. 5. Total leakage current as a function of elapsed time. The source was on during the time indicated by the arrows. The bias voltage of SII sensors was changed in the last irradiation period as shown in the plot.

four sensors were noted as frequently as shown in the plot with that of the fourth sensor (SII #12) being recorded automatically. Right after the source was set, all the sensors showed roughly the same leakage current of $\sim 70 \mu\text{A}$ which is due to the ionization by the source. The sensors of the same manufacturer behaved similarly, but the SII sensors showed a steep increase during the irradiation while the HPK sensors showed a constant but small increase over the irradiation period. The bias voltage of the SII sensors was lowered from 55 to 45 V midpoint in the last irradiation period while that of HPK sensors was kept at 120 V. The excellent behavior of HPK sensors is due to the superior design of the edge n^+ implants and Al metallization on top.

The I - V curve was measured typically 10–30 min after the source was removed. Fig. 6 shows the I - V curves of HPK sensor #12. The onset voltage of micro-discharge shifted from 180 to 130 V by irradiation. The charge accumulation in the oxide layers is attributed to this change, which enhances the electric field near the p^+ implants. Another HPK sensor showed essentially the same effects but the shift of the onset voltage was about 20 V. The shift in the SII sensors was not visible because of the large leakage through the edges.

After the irradiation, the sensors were brought to the University of Tsukuba where the sensors were kept biased at a temperature of 20°C . The total

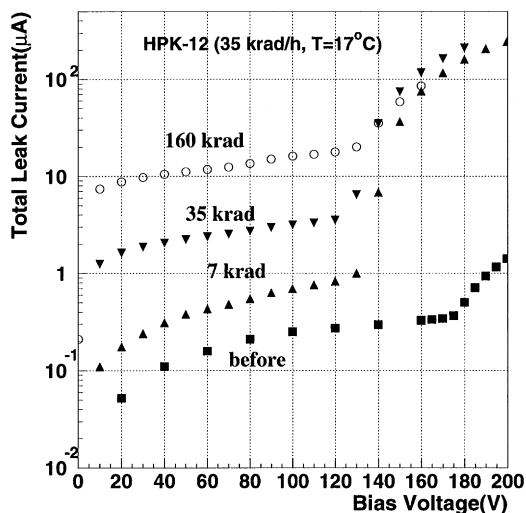


Fig. 6. Leakage current of HPK #12 sensor, measured right after the ^{60}Co source was removed. The number attached to each curve is the accumulated dose.

leakage current decreased by about an order of magnitude in a day but nearly saturated thereafter; the leakage current decreased by 21% (7%) for HPK sensors and by 37% (28%) for SII sensors when we compare the current one day (three days) after the irradiation to that one week after.

The I - V characteristics measured before and one week after the irradiation are shown in Fig. 7 for the four samples. The HPK leakage current at the operation voltage was about one order smaller than our specification of $120 \mu\text{A}$ while the SII leakage current was below but close to the specification. Both of the tested SII sensors had the onset voltage of micro-discharge at rather low voltages before irradiation. We have conducted another irradiation test of sample SII #01, one of the sensors with best I - V characteristics (see Fig. 2), but we found it behave similarly to the two SII sensors shown in Fig. 7.

The strip current of one of the irradiated SII sensors was measured six months after the irradiation. The results are plotted in Fig. 8. The leakage current of quiet strips ranges from 50 to 60 nA at 100 V while it was about 10 nA before irradiation. We note that the strip leakage current increases gradually with bias voltage even above the full

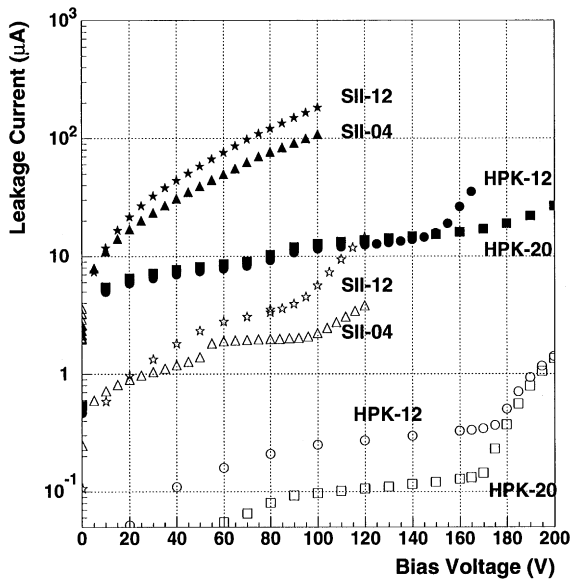


Fig. 7. The total leakage current as a function of the bias voltage (open marks) before and (solid marks) one week after the irradiation of 0.16 Mrad.

depletion voltage whereas a plateau is visible above the full depletion voltage for HPK sensors.

The mobility of ions in insulator materials is small and radiation-induced ions could be accumulated in insulator layers, which could influence the interstrip capacitance. On the n-side the accumulation layer effectively interconnects the strips and hence higher bias voltages are necessary to minimize the interstrip capacitance. The interstrip capacitances on n-side and p-side were measured before and one week after the irradiation, which are shown in Figs. 9 and 10 for HPK and SII sensors. The capacitance was measured at 1 MHz. After the irradiation, the bias voltage had to be raised by ~ 5 V for HPK and ~ 20 V for SII in order to accomplish necessary n strip isolation. As described before, additional silicon nitride layer degrades the leakage current characteristics. It can also be concluded that additional silicon nitride passivation layer affects the interstrip capacitance change more severely.

Silicon nitride such as in the MNOS (metal-Si₃N₄-SiO₂-Si) devices is used for the purpose of reducing the interface-trap density by

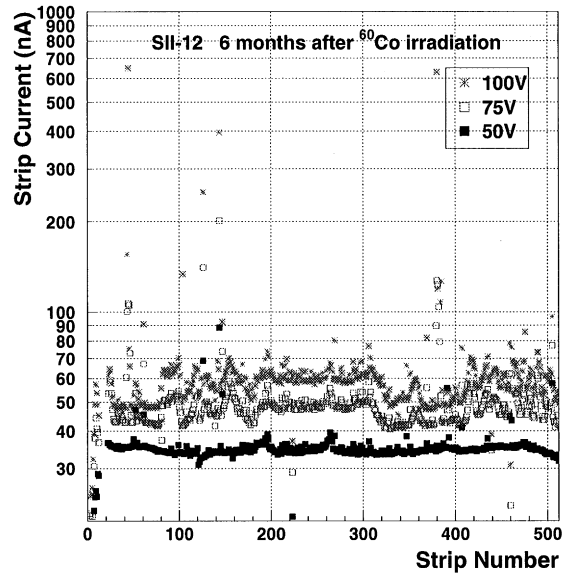


Fig. 8. Strip leakage current of irradiated SII sensor measured six months after the irradiation of 0.16 Mrad. The bias voltages are 50, 75 and 100 V.

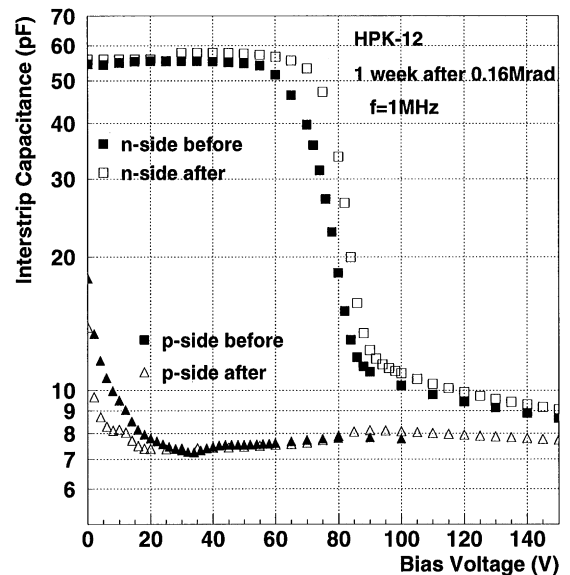


Fig. 9. Interstrip capacitance of HPK sensor measured before and after irradiation.

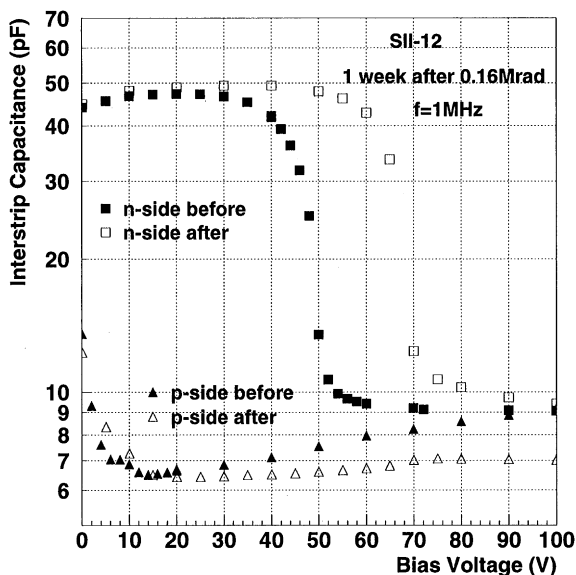


Fig. 10. Interstrip capacitance of SII sensor measured before and after irradiation.

making a clean SiO_2 -Si interface and of preventing (Na) ions to migrate by the outer Si_3N_4 film [18]. Also the conductivity of silicon nitride is orders of magnitude higher than SiO_2 . From these arguments, we naively expect a better performance because of fewer oxide charges which include the interface-trap charges, oxide-trap charges, mobile ionic charges and fixed oxide charges [18]; change in the sum of these charges should affect the interstrip capacitance. The function of the Si_3N_4 - SiO_2 interface possibly explains the observation. In MNOS memory devices, although metal ions are doped into SiO_2 to form the interfacial charge storage centers, the Si_3N_4 - SiO_2 interface can store charges [18]. At specific conditions such devices can hold charges extending to 100 years.

4. Summary

Prototype double-sided Si microstrip sensors were fabricated for the CDF-II ISL detector. The sensors were manufactured by Hamamatsu Photonics and SEIKO Instruments using 4" technology. The major differences in the design are the structure

of the coupling capacitors and the passivation. SII sensors have silicon nitride passivation while HPK sensors have SiO_2 .

Both HPK and SII sensors satisfied the leakage current requirements that the total current at the operation voltage be less than $4 \mu\text{A}$ ($100 \text{ nA}/\text{cm}^2$). The leakage current of HPK sensors is, though, a factor of 10 smaller than that of SII sensors. Most of the strips showed small leakage currents of 1–10 nA while some strips showed larger currents. These strips are responsible for the steep increase in the total leakage current, which is typically 80 V and 50 V above the full depletion voltage for HPK and SII sensors, respectively.

The quality of the surface was compared using ^{60}Co γ -rays. The leakage current at the operation voltages increased by a factor of 40–100 one week after 0.16 Mrad irradiation, which however are within our specification. The increase in the leakage current, which is explained by charge accumulation in insulation layers and/or at interfaces, remains at least for months for SII sensors. The bias voltage necessary to minimize the interstrip capacitance is shifted after the irradiation. SII sensors showed a larger shift of 20 V whereas HPK sensors showed a shift of 5 V.

Acknowledgements

We would like to appreciate K. Yamamura of Hamamatsu Photonics, and Y. Saitoh and T. Akamine of SEIKO Instruments for discussions on the sensor design. This work is supported in part by a Grant-in Aid from the Japanese Ministry of Education, Science and Culture.

References

- [1] CDF II Collaboration, Technical Design Report, FER-MILAB-Pub-96/390-E, November 1996.
- [2] T. Ohsugi et al., Nucl. Instr. and Meth. A 342 (1994) 16.
- [3] T. Ohsugi et al., Nucl. Instr. and Meth. A 383 (1996) 116.
- [4] E. Barberis et al., Nucl. Instr. and Meth. A 342 (1994) 90.
- [5] J.F. Krizmanic, Nucl. Instr. and Meth. A 342 (1994) 27.
- [6] P.I. Hopman et al., Nucl. Instr. and Meth. A 383 (1996) 98.
- [7] T. Ohsugi et al., Nucl. Instr. and Meth. A 342 (1994) 16.
- [8] R. Wheadon et al. (RD20), Nucl. Instr. and Meth. A 348 (1994) 449.

- [9] J. Matheson et al. (RD20), Nucl. Instr. and Meth. A 362 (1995) 297.
- [10] T. Zimmerman et al., IEEE Trans. Nucl. Sci. NS-40 (4) (1993) 736.
- [11] P.W. Nicholson, Nuclear Electronics, Wiley, New York, 1974.
- [12] Y. Saitoh et al., Nucl. Instr. and Meth. A 342 (1994) 186.
- [13] S. Okuno et al., Nucl. Instr. and Meth. A 361 (1995) 91.
- [14] H. Ikeda et al., Nucl. Instr. and Meth. A 376 (1996) 155.
- [15] S.C. Seidal et al., Nucl. Instr. and Meth. A 383 (1996) 128.
- [16] Y. Saitoh et al., IEEE Trans. Nucl. Sci. NS-43 (1996) 1123.
- [17] See, for example, a summary by G.N. Taylor et al., Nucl. Instr. and Meth. A 383 (1994) 144.
- [18] S.M. Sze, Physics of Semiconductor Devices, Wiley, New York, 1981.